Original article

Challenges in mathematical modeling of dynamic mass transfer controlled by capillary and viscous forces in spontaneous fluid imbibition processes

Md Nahin Mahmood[ORCID]*, Vu Nguyen, Boyun Guo

Department of Petroleum Engineering, University of Louisiana at Lafayette, Lafayette 70503, USA

Abstract:
Dynamic mass transfer due to spontaneous imbibition is of significant importance in various scientific and engineering applications, including environmental remediation, chemical reactors, microfluidic systems, and oil recovery processes. This article addresses the challenges in mathematical modeling of the dynamic mass transfer due to spontaneous imbibition controlled by capillary and viscous forces. A mathematical model was developed to seamlessly integrate the effects of capillary and viscous forces on mass transfer. The model was validated by comparison with numerical solution, which shows excellent consistency, indicating no error in the derivation of the analytical model. Case analysis suggested some limitations of the analytical model. The model does not work at the starting point of imbibition because of mathematical singularity. The current computing technology does not generate model results under all conditions due to the data-overflow issue associated with the exponential function involved in the analytical model. Although using numerical solution with finite difference method can eliminate the data-overflow problem, time step size must be small enough to achieve algorithm convergence and generate meaningful result.

1. Introduction

Spontaneous imbibition is the process by which a wetting fluid is drawn into a porous medium by capillary action. The transport of mass in fluid systems is inherently governed by the interplay of various forces, three of the most significant being capillary, gravitational, and viscous forces. In horizontal mass transfer processes, the effect of gravity is null, and the mass transfer rate is dominated by capillary and viscous forces. Capillary forces arise due to the surface tension of liquids, leading to phenomena such as capillary rise, droplet formation, and wetting behavior (Bear, 2013). Viscous forces, on the other hand, are associated with the resistance to fluid flow and are influenced by the viscosity of the fluid transferring mass (Bear, 1975, 2013). Mass transfer in porous media, characterized by the movement of substances through intercon-

nected void spaces, is a complex and pervasive phenomenon with significant implications for various fields, including hydrogeology, environmental science, and petroleum recovery processes (Levenspiel, 1998). In such media, the interplay between capillary and viscous forces plays a crucial role in governing spontaneous fluid imbibition processes. Capillary forces, driven by the surface tension of liquids, play a pivotal role in capillary rise and simultaneous imbibition processes. Viscous forces, on the other hand, are associated with fluid flow resistance and impact the rate of mass transport through the porous medium. The weight of wetting liquid imbibed into porous media is a function of contact area, porosity, pore fractal dimension, tortuosity, maximum hydraulic pore diameter, liquid density, viscosity, surface tension and liquid-solid interactions (Cai et al., 2012).

Pore-scale studies of spontaneous imbibition can help us

disclose the underlying physics of imbibition mechanisms, and fill the gap between pore-scale dynamics and the Darcy theory of spontaneous imbibition. Presently, the temporal resolution limits of existing noninvasive visualization techniques prevent us from fully displaying the dynamic displacements of phases at the pore-scale in a genuine three-dimension porous media (Bartels et al., 2019), especially for cocurrent spontaneous imbibition. Therefore, the utilization of pore-scale modeling could yield significant advantages (Chen et al., 2022). Thus far, popular pore-scale numerical models have been used to study spontaneous imbibition (SI) like Volume-of-Fluid models, Lattice-Boltzmann models, phase-filed models, and dynamic pore-network models (Qin, 2015; Raeini et al., 2015; Rokhforouz and Amiri, 2018; Zheng et al., 2018; Bakhshian et al., 2020; Zhao et al., 2020; Diao et al., 2021). The dynamic pore network model is particularly notable for its computational efficiency (Blunt et al., 2013).

As a fundamental mass transfer process, the importance of spontaneous imbibition mechanism has long been recognized in many hydrological and geotechnical applications, such as sequestration of carbon dioxide (Plug and Bruining, 2007; Prather et al., 2016; Lyu et al., 2020), oil and gas extraction (Standnes, 2010; Gao and Hu, 2016; Zhou et al., 2016), and the protection of groundwater resources (Jiménez-Martínez et al., 2020). In the early-time stage, the SI process is capillary dominated and the influence of gravity might be overlooked because of the insignificant amount of imbibed water. Nevertheless, the early-stage spontaneous imbibition process in fractured porous media, particularly in dual-porosity media containing both matrix and filled fractures, remains intricate and inadequately comprehended, mostly due to the widespread variety of geologic formations (Zhao et al., 2020).

Extensive research has been conducted in recent decades using experimental and theoretical methods to study the behavior of spontaneous imbibition. These studies have revealed that the rate at which imbibition occurs, which measures the mass transfer during the process, is influenced by factors such as pore structure, fluid properties, initial water saturation, boundary conditions, and mineralization (Morrow and Mason, 2001; Gao and Hu, 2016; Lyu et al., 2019).

Several sophisticated mathematical models have been suggested to investigate and describe the SI mechanism. Pioneering models for the spontaneous imbibition process includes the Handy model, the Lucas-Washburn model, and the Aronofsky model (Dou et al., 2022). Over the past few decades, advancements have been made in developing models that represent a pore system at multiple scales. These models have been enhanced by including a shape factor to consider the influence of pore sizes and shapes. Cai and Yu (2011) developed an analytical model using the Lucas-Washburn model to examine the impact of tortuosity on capillary imbibition in wet porous media, specifically focusing on the fractal dimension of tortuous capillaries. Subsequently, Cai et al. (2014) developed a comprehensive model for spontaneous imbibition, using the Hagen-Poiseuille and Laplace-Young equations. This model takes into consideration the influence of tortuous capillaries and noncircular cross-sectional geometries by incorporating variably shaped pores. Ashraf and Phirani (2019b) devised

a comprehensive lubrication approximation model to forecast the wetting front in a horizontally multi-layered porous medium during the SI process. Their model, based on the Washburn model, revealed that the wetting front's location was not consistently within the fine pores. Instead, it was heavily influenced by variations in permeability and capillary pressure. This outcome aligns with their prior discoveries and suppositions (Ashraf et al., 2017; Ashraf and Phirani, 2019a). Li et al. (2016) developed a complex fractal model to estimate the permeability of a dual-porosity medium with randomly dispersed fractures. The accuracy of the fractal aperture distribution was confirmed by comparing it to the in-situ measurement findings documented in existing literature. In their study, Dou et al. (2022) conducted both experimental and theoretical investigations on the process of solute infiltration in a medium with two distinct porosities: The matrix and the filled crack. The findings indicated that the rate of matrix imbibition was higher in the dual-porosity media compared to the single-porosity media. The discrepancy in the rate of liquid absorption between the media with a single porosity and those with dual porosity was due to the improved transfer of mass between the matrix and the crack that was filled. The research was analyzed either qualitatively or quantitatively with regards to the kinetics of capillary absorption for the solvent impregnation process.

In microfluidic systems and lab-on-a-chip devices, where dimensions are in the order of micrometers, capillary and viscous forces govern fluid behavior and mass transport, impacting applications such as chemical analysis, medical diagnostics, and drug delivery (Stone and Kim, 2001; Squires and Quake, 2005). In chemical reactors, the control of mass transfer is paramount for optimizing reaction rates, and the interaction between capillary and viscous forces becomes particularly challenging in non-ideal reactor configurations (Levenspiel, 1998; Bird et al., 2002). Environmental processes, including groundwater remediation and contaminant transport, also display the significance of capillary and viscous forces. The movement of pollutants through porous media is intricately tied to these forces, influencing the efficacy of remediation strategies (Lichtner, 1985; Bear, 2013). Therefore, a comprehensive understanding of these forces is indispensable for addressing environmental challenges and ensuring sustainable resource management.

Porous media, encompassing soils, rocks, and engineered materials, constitute a common substrate for mass transfer phenomena. The porous structure provides interconnected void spaces through which fluids and solutes can migrate, making it a critical medium for various applications. Spontaneous fluid imbibition in porous media is a key consideration in environmental applications, particularly in groundwater remediation and contaminant transport. Understanding how capillary and viscous forces influence the movement of pollutants is crucial for designing effective remediation strategies. The work of Bear (1975) laid the foundation for conceptualizing fluid flow and mass transfer in porous media, providing a theoretical framework that has since guided research in the field.

Despite the importance of understanding spontaneous fluid imbibition in porous media, the development of accurate
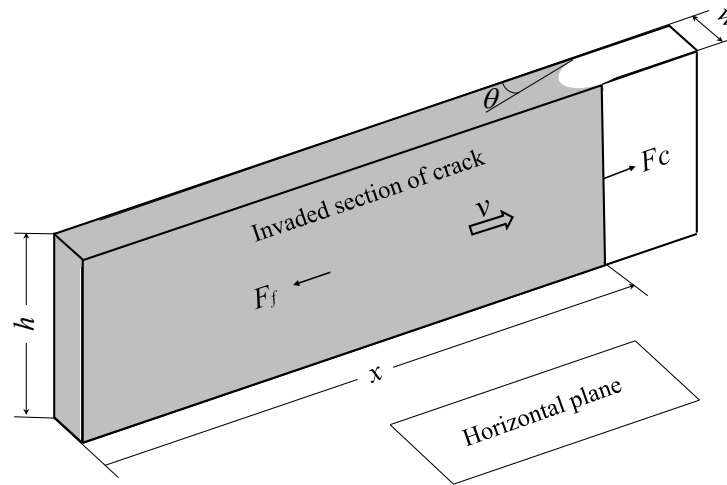
Fig. 1. A sketch to define mass transfer into a crack of rectangular cross-section.

mathematical models faces several challenges. Cai et al. (2014) formulated a generalized model that can be used to characterize the spontaneous imbibition behavior of many different porous media and that pore shape cannot always be assumed to be cylindrical. Latest multi-scale simulation and experimental methods to study multi-field coupling problems in complex porous media were investigated by Yang et al. (2021). The porous structure introduces complexities such as heterogeneity, anisotropy, and variability in pore sizes, making it challenging to derive universal models applicable across different media. The need for models that can account for these variations while capturing the interplay between capillary and viscous forces remains a critical research gap (Berkowitz, 2002). Non-linearity is another significant challenge in mathematical modeling, especially when considering the impact of dynamic processes on mass transfer. The transition from immobile to mobile fluid phases and the associated changes in pore saturation levels introduce non-linearities that complicate the derivation of predictive models. This challenge is further compounded by the need to integrate capillary and viscous forces seamlessly. The transient nature of mass transfer events in porous media adds an additional layer of complexity. Processes such as solute transport during rainfall events or contaminant release from industrial sites involve dynamic interactions between capillary and viscous forces. Developing mathematical models that can accurately capture the transient behavior of mass transfer in response to changing environmental conditions is an open problem with great challenge.

Spontaneous imbibition processes in tight porous media have been studied in recent years, mainly focusing on laboratory experiments, theoretical analysis, and numerical simulations. Cai et al. (2023) provides a summary of the most recent advances in the studies of capillary behavior in shale gas/oil reservoirs, showing the challenge in modeling of the spontaneous imbibition due to the complex imbibition mechanism. Owing to the multi-influencing factors such as petrophysical properties of shales and fluid properties, it is difficult to understand thoroughly the microscopic and macroscopic flow mechanisms in spontaneous imbibition processes.

Published literature indicates several critical research gaps in the mathematical modeling of spontaneous fluid imbibition in porous media. Firstly, there is a pressing need for models that seamlessly integrate both capillary and viscous forces, recognizing the intricate interplay between these two phenomena. Existing models often treat these forces separately, limiting their applicability in scenarios where both forces act simultaneously. Secondly, the development of mathematical models that can accommodate external factors, such as temperature variations or chemical reactions, is essential for real-world applications. The literature in public domain suggests a gap in understanding how these external factors influence the interplay between capillary and viscous forces, adding complexity to the modeling task. Thirdly, experimental validation of theoretical models is crucial for establishing their reliability and applicability. While mathematical models offer valuable insights, experimental verification is necessary to bridge the gap between theoretical predictions and real-world scenarios. Integrating these experimental data into mathematical models can enhance the accuracy of predictions and provide insights into the role of capillary and viscous forces in dynamic mass transfer due to spontaneous imbibition (Wildenschild et al., 2002). Employing analytical models calibrated with laboratory data confers numerous advantages in enhancing the accuracy and reliability of simulations across scientific and engineering domains. Calibration with experimental data ensures that analytical models accurately represent the intricacies of real-world phenomena. This process allows for fine-tuning model parameters to align with empirical observations, significantly improving predictive capabilities (Kleijnen, 2018). The integration of laboratory data facilitates rigorous validation and verification, establishing the credibility of the model outcomes (Saltelli et al., 2008). Additionally, calibrated analytical models provide a cost-effective and time-efficient means of understanding complex systems, optimizing designs, and informing decision-making in diverse applications. As a result, the combination of analytical modeling and laboratory data contributes to more robust and applicable solutions in fields ranging from environmental science to engineering.
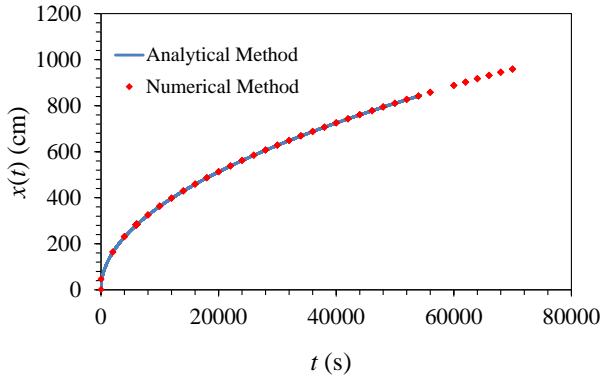
Fig. 2. Comparison of analytical and numerical solutions.

Addressing the open problem of mathematical modeling of dynamic mass transfer in spontaneous fluid imbibition processes governed by the capillary and viscous forces, this paper presents an analytical model with numerical validation. The model was analyzed in sensitivity analysis to identify its limit to real world applications. It was found that due to the nature of the governing equation with singularity, the solution does not work at location zero. The shortest distance from the starting point for the model to work depends on the data-overflow limit in evaluation of the exponential function involved in the analytical model. Numerical solution of the governing equation converges with low values of time step size.

2. Mathematical model

Natural micro-mass transfer is induced by capillary force and resisted by viscous force in capillary space. The mass transfer process can be affected by gravitational force, depending on orientation of motion. The capillary force (F_c) can be formulated based on interfacial tension (σ), contact angle (θ) and perimeter of capillary. It is customary to express the capillary force as a function of capillary pressure (p_c) through capillary area (A):

$$F_c = Ap_c \tag{1}$$

The cross-sectional areas for capillaries having cross-sections of rectangular shape (Fig. 1), circular shape with radius r_c, and elliptical shape with radii of curvature r_1 and r_2, the capillary areas are hw, πr_c^2 and $\pi r_1 r_2$, respectively.

For capillaries having cross-sections of rectangular shape, the capillary pressure is expressed as (Zhang et al., 2021):

$$p_c = \frac{2\sigma\cos\theta}{hw}(h+w) \tag{2}$$

For capillaries having cross-sections of circular shape, the capillary pressure is expressed as (Young, 1832):

$$p_c = \frac{2\sigma\cos\theta}{r_c} \tag{3}$$

For capillaries having cross-sections of elliptical shape, the capillary pressure is expressed as (Laplace and Marquis de, 1805):

$$p_c = \sigma\cos\theta\left(\frac{1}{r_1}+\frac{1}{r_2}\right) \tag{4}$$

Frictional force here refers to the resistance to flow of fluid due to the interactions between fluid and tube wall and inter-particles in viscous systems. The flow frictional force F_f acting on the invading (wetting) phase over an invading penetration length x is expressed as:

$$F_f = Ap_f \tag{5}$$

where the friction pressure p_f is expressed as (Faber, 2021):

$$p_f = \frac{f_f\rho v^2 x}{d_H} \tag{6}$$

where ρ is fluid density, f_f is friction factor, v is the average fluid velocity, and d_H is hydraulic diameter of the capillary and x is the distance travelled during fluid flow.

Assuming laminar flow the friction factor is expressed as:

$$f_f = \frac{16}{N_{Re}} \tag{7}$$

where the Reynolds number N_{Re} is given by:

$$N_{Re} = \frac{d_H\rho v}{\mu} \tag{8}$$

where μ is fluid viscosity.

Substituting Eqs. (7) and (8) into Eq. (6) gives:

$$p_f = \frac{16\mu vx}{d_H^2} \tag{9}$$

For horizontal imbibition processes where gravity effect is zero, applying Newton's second law of motion to the flowing fluid gives:

$$F_c - F_f = \rho Ax\frac{dv}{dt} \tag{10}$$

Substitutions of Eqs. (1) and (5) into Eq. (10) yield for flow in the pore space:

$$Ap_c - Ap_f = \rho Ax\frac{dv}{dt} \tag{11}$$

Substitutions of Eq. (9) into Eq. (11) yield:

$$p_c - \frac{16\mu vx}{d_H^2} = \rho x\frac{dv}{dt} \tag{12}$$

Because $v = dx/dt$, Eq. (12) is rearranged to give:

$$\frac{d^2x}{dt^2} + A\frac{dx}{dt} + \frac{B}{x} = 0 \tag{13}$$

where:

$$A = \frac{16\mu}{\rho d_H^2} \tag{14}$$

$$B = -\frac{p_c}{\rho} \tag{15}$$

Eq. (13) can be solved using the following initial conditions:

$$x = x_0 \quad \text{at} \quad t = 0 \tag{16}$$

The initial velocity is generally zero if the time is counted

Table 1. Basic data used in a model comparison.

Parameter	Value	Unit
Capillary pressure (p_c)	105	dyne/cm^2
Viscosity of fluid (μ)	0.01	poise
Hydraulic diameter (d_H)	0.0001	cm
Time (t)	0 to 86,400	s
Initial location (x_0)	1	cm
Initial velocity (v_0)	1	cm/s

Fig. 3. Numerical solution results for different time step sizes.

from the original point. The model allows for using non-zero value if the value is specified from a point other than the origin. This makes the model general for more application scenarios. Therefore, we use the initial condition expressed as:

$$\frac{\mathrm{d}x}{\mathrm{d}t} = v_0 \quad \text{at} \quad t = 0 \tag{17}$$

The analytical solution for Eq. (13) takes the following parametric form (see Appendix A for derivation):

$$x(v) = -\frac{A e^{-\frac{Av^2}{2}}}{B\left(C + \int_0^v e^{-\frac{Av^2}{2}}\,\mathrm{d}v\right)} \tag{18}$$

where the integral relates to time t by:

$$t(v) = \frac{A}{B^2}\ln\left(C + \int_0^v e^{-\frac{Av^2}{2}}\,\mathrm{d}v\right) + C^* \tag{19}$$

where the integral can be evaluated using error function expressed by:

$$\mathrm{erf}\left(\sqrt{\frac{A}{2}}v\right) = \frac{2}{\sqrt{\pi}}\int_0^v e^{-\frac{Av^2}{2}}\,\mathrm{d}v \tag{20}$$

where C and C^* are integration constants determined by the initial conditions.

To ensure that the derivation of the analytical solution has no error, the analytical solution was validated by numerical solution of the governing Eq. (13) subjected to the initial conditions expressed by Eqs. (16) and (17). The numerical solution was obtained using the finite difference method (FDM) formulated in Appendix B. Data in Table 1 was employed to generate results from the analytical and numerical solutions. A comparison of the solutions is presented in Fig. 2. An excellent consistency of the two solutions is observed, indicating no error was introduced in the derivation of the analytical solution.

Fig. 2 illustrates the result of both analytical solution of the model along with its validation by numerical method. It depicts a super consistency of the two solutions as both the curves overlap each other, indicating no error was introduced in the derivation of the analytical solution.

3. Challenges in model applications

The analytical solution was found difficult to use in some conditions. First, the model does not work at the starting point because of the singularity of Eq. (1) at $x = 0$. Secondly, in some cases, the current computing technology does not gen-
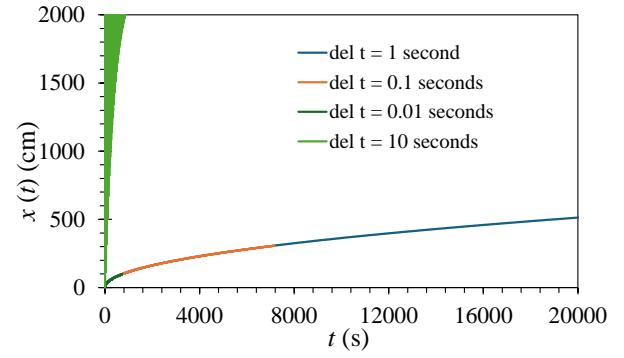
erate solution result due to the data overflow in the exponential function involved in the solution form. For the data set in Table 1, the value of the coefficient A in Eq. (1) has to be less than or equal to 852 ($A \leq 852$) to generate solution result.

There are several numerical methods that can be used to solve Eq. (13). Forward Euler's Method is one of them which takes the general form:

$$x_{n+1} = x_n + h_1 f(t_n, x_n) \tag{21}$$

where x_{n+1} is value of "x" at next time step, x_n is value of "x" at current time step, h_1 is step-size, $f(t_n, x_n)$ is derivative function of time t_n and x_n.

Here, there is a second order ordinary differential equation which can be converted into first order ordinary differential equation by a new variable, $v = \mathrm{d}x/\mathrm{d}t$. Then Eq. (13) turns into:

$$\frac{\mathrm{d}v}{\mathrm{d}t} = -Av - \frac{B}{x} \tag{22}$$

Applying Forward Euler's Method:

$$x_{n+1} = x_n + h_1 v_n \tag{23}$$

$$v_{n+1} = v_n + h_1\left(-Av_n - \frac{B}{x_n}\right) \tag{24}$$

where, v_{n+1} and v_n are the velocities at different time-steps.

To analyze stability, let's introduce the "Amplification Factor" x_{n+1}/x_n is introduced. Substituting Eqs. (23) and (24) for x_{n+1} and v_{n+1} with amplification factor gives:

$$\frac{x_{n+1}}{x_n} = 1 + h_1\frac{v_n}{x_n} \tag{25}$$

and:

$$\frac{v_{n+1}}{v_n} = 1 - h_1\left(A - \frac{h_1 B}{x_n v_n}\right) \tag{26}$$

Therefore, the numerical stability criterion is as follows:

$$\left|1 + h_1\frac{v_n}{x_n}\right| \leq 1 \tag{27}$$

or:

$$\left|1 - h_1\left(A - \frac{h_1 B}{x_n v_n}\right)\right| \leq 1 \tag{28}$$

For calculation finite difference method is used here. Use of numerical solution approach with FDM can eliminate the second problem of the analytical method. However, the time

step size must be small enough to generate results if an explicit algorithm is employed. Fig. 3 presents numerical solution result for different values of time-step size (Δt). It shows that all the curves overlap with each other when the time-step size is less than or equal to 1 second, while the solution algorithm does not converge for $\Delta t = 10$ seconds.

4. Conclusions

A governing equation for mass transfer processes dominated by capillary and viscous forces in spontaneous fluid imbibition was formulated. An analytical solution was obtained with initial conditions. The following conclusions are drawn.

1) The analytical solution was validated by comparison with numerical solution. The results given by the two solutions are highly consistent, indicating no error in the derivation of the analytical solution.

2) There are two challenges in using the analytical solution. First, the solution does not work at the starting point because of mathematical singularity. This means that solving the equation for the mass transfer rate near the starting point may give some error, depending on the distance from the starting point. Secondly, in some cases, the current computing technology does not generate solution results due to the data-overflow issue in the exponential function involved in the solution form.

3) Use of numerical solution with FDM can eliminate the data-overflow problem of the analytical solution. However, the time step size must be small enough to generate result. The criterion for selection of the maximum stable time-step size should be applied to achieving stable algorithm for improving computing efficiency.

4) Future work should include validation of the analytical solution through comparisons with experimental data and/or previous solutions.

Acknowledgements

Conflict of interest

The authors declare no competing interest.

References

Ashraf, S., Phirani, J. Capillary displacement of viscous liquids in a multi-layered porous medium. Soft Matter, 2019a, 15(9): 2057-2070.

Ashraf, S., Phirani, J. A generalized model for spontaneous imbibition in a horizontal, multi-layered porous medium. Chemical Engineering Science, 2019b, 209: 115175.

Ashraf, S., Visavale, G., Bahga, S. S., et al. Spontaneous imbibition in parallel layers of packed beads. The European Physical Journal E, 2017, 40: 1-6.

Bakhshian, S., Rabbani, H. S., Hosseini, S. A., et al. New insights into complex interactions between heterogeneity and wettability influencing two-phase flow in porous media. Geophysical Research Letters, 2020, 47(14): e2020GL088187.

Bartels, W. B., Rücker, M., Boone, M., et al. Imaging spontaneous imbibition in full Darcy-scale samples at pore-scale resolution by fast X-ray tomography. Water Resources Research, 2019, 55(8): 7072-7085.

Bear, J. Dynamics of fluids in porous media. Soil Science, 1975, 120: 162-163.

Bear, J. Dynamics of Fluids in Porous Media. New York, USA, Dover Publications, 2013.

Berkowitz, B. Characterizing flow and transport in fractured geological media: A review. Advances in Water Resources, 2002, 25(8-12): 861-884.

Bird, R. B., Stewart, W. E., Lightfoot, E. N. Transport Phenomena. New York, USA, John Wiley & Sons, 2002.

Blunt, M. J., Bijeljic, B., Dong, H., et al. Pore-scale imaging and modelling. Advances in Water Resources, 2013, 51: 197-216.

Cai, J., Hu, X., Standnes, D. C., et al. An analytical model for spontaneous imbibition in fractal porous media including gravity. Colloids and Surfaces A: Physicochemical and Engineering Aspects, 2012, 414: 228-233.

Cai, J., Perfect, E., Cheng, C. L., et al. Generalized modeling of spontaneous imbibition based on Hagen-Poiseuille flow in tortuous capillaries with variably shaped apertures. Langmuir, 2014, 30(18): 5142-5151.

Cai, J., Sun, S., Wang, H. Current advances in capillarity: Theories and applications. Capillarity, 2023, 7(2): 25-31.

Cai, J., Yu, B. A discussion of the effect of tortuosity on the capillary imbibition in porous media. Transport in Porous Media, 2011, 89(2): 251-263.

Chen, L., He, A., Zhao, J., et al. Pore-scale modeling of complex transport phenomena in porous media. Progress in Energy and Combustion Science, 2022, 88: 100968.

Diao, Z., Li, S., Liu, W., et al. Numerical study of the effect of tortuosity and mixed wettability on spontaneous imbibition in heterogeneous porous media. Capillarity, 2021, 4(3): 50-62.

Dou, Z., Zhao, Y., Wei, Y., et al. Enhanced mass transfer between matrix and filled fracture in dual-porosity media during spontaneous imbibition based on low-field nuclear magnetic resonance. Journal of Hydrology, 2022, 607: 127521.

Faber, T. E. Fluid Dynamics for Physicists. Cambridge University Press, Cambridge, 1995.

Gao, Z., Hu, Q. Initial water saturation and imbibition fluid affect spontaneous imbibition into Barnett shale samples. Journal of Natural Gas Science Engineering, 2016, 34, 541-551.

Jiménez-Martínez, J., Alcolea, A., Straubhaar, J. A., et al. Impact of phases distribution on mixing and reactions in unsaturated porous media. Advances in Water Resources, 2020, 144: 103697.

Kleijnen, J. P. C. Design and analysis of simulation experiments, in Statistics and Simulation, edited by J. Pilz, D. Rasch, V. B. Melas et al., Springer International Publishing, Cham, pp. 3-22, 2018.

Laplace, Marquis de, P. S. Traité de Mécanique Celeste. Paris, France, Chez J.B.M. Duprat, 1805.

Levenspiel, O. Chemical Reaction Engineering. New York, USA, John Wiley & Sons, 1998.

Li, B., Liu, R., Jiang, Y. A multiple fractal model for estimating permeability of dual-porosity media. Journal of Hydrology, 2016, 540: 659-669.

Lichtner, P. C. Continuum model for simultaneous chemical reactions and mass transport in hydrothermal systems. Geochimica et Cosmochimica Acta, 1985, 49(3): 779-800.

Lyu, C., Ning, Z., Chen, M., et al. Experimental study of boundary condition effects on spontaneous imbibition in tight sandstones. Fuel, 2019, 235: 374-383.

Lyu, Q., Wang, K., Wanniarachchi, W. A. M., et al. Hydro-mechanical properties of a low-clay shale with supercritical CO_2 imbibition. Geomechanics and Geophysics for Geo-Energy and Geo-Resources, 2020, 6(4): 69.

Morrow, N. R., Mason, G. Recovery of oil by spontaneous imbibition. Current Opinion in Colloid & Interface Science, 2001, 6(4): 321-337.

Plug, W. J., Bruining, J. Capillary pressure for the sand-CO_2-water system under various pressure conditions. Application to CO_2 sequestration. Advances in Water Resources, 2007, 30(11): 2339-2353.

Prather, C. A., Bray, J. M., Seymour, J. D., et al. NMR study comparing capillary trapping in Berea sandstone of air, carbon dioxide, and supercritical carbon dioxide after imbibition of water. Water Resources Research, 2016, 52(2): 713-724.

Qin, C. Water transport in the gas diffusion layer of a polymer electrolyte fuel cell: Dynamic pore-network modeling. Journal of the Electrochemical Society, 2015, 162(9): F1036.

Raeini, A. Q., Bijeljic, B., Blunt, M. J. Modelling capillary trapping using finitevolume simulation of two-phase flow directly on micro-CT images. Advances in Water Resources, 2015, 83: 102-110.

Rokhforouz, M. R., Amiri, H. A. Pore-level influence of micro-fracture parameters on visco-capillary behavior of two-phase displacements in porous media. Advances in Water Resources, 2018, 113: 260-271.

Saltelli, A., Ratto, M., Andres, T., et al. Global Sensitivity Analysis: The Primer. New York, USA, John Wiley & Sons, 2008.

Squires, T. M., Quake, S. R. Microfluidics: Fluid physics at the nanoliter scale. Reviews of Modern Physics, 2005, 77(3): 977.

Standnes, D. C. Scaling spontaneous imbibition of water data accounting for fluid viscosities. Journal of Petroleum Science Engineering, 2010, 73(3-4): 214-219.

Stone, H. A., Kim, S. Microfluidics: Basic issues, applications, and challenges. AIChE Journal, 2001, 47(6): 1250.

Wildenschild, D., Vaz, C. M. P., Rivers, M. L., et al. Using X-ray computed tomography in hydrology: Systems, resolutions, and limitations. Journal of Hydrology, 2002, 267(3-4): 285-297.

Yang, Y., Zhou, Y., Blunt, M. J., et al. Advances in multiscale numerical and experimental approaches for multiphysics problems in porous media. Advances in Geo-Energy Research, 2021, 5(3): 233-238.

Young, T. An essay on the cohesion of fluids, in Philosophical Transactions of the Royal Society of London, edited by T. Young, The Royal Society London, London, pp: 65-87, 1832.

Zhang, P., Guo, B., Liu, N. Numerical simulation of CO_2 migration into cement sheath of oil/gas wells. Journal of Natural Gas Science and Engineering, 2021, 94: 104085.

Zhao, J., Qin, F., Derome, D., et al. Simulation of quasi-static drainage displacement in porous media on pore-scale: Coupling lattice Boltzmann method and pore network model. Journal of Hydrology, 2020, 588: 125080.

Zheng, J., Ju, Y., Wang, M. Pore-scale modeling of spontaneous imbibition behavior in a complex shale porous structure by pseudopotential lattice Boltzmann method. Journal of Geophysical Research: Solid Earth, 2018, 123(11): 9586-9600.

Zhou, Z., Abass, H., Li, X., et al. Experimental investigation of the effect of imbibition on shale permeability during hydraulic fracturing. Journal of Natural Gas Science Engineering, 2016, 29: 413-430.

Appendix A. Analytical solution for mass transfer in spontaneous imbibition processes

For the governing equation in form of

$$\frac{d^2x}{dt^2} + A\frac{dx}{dt} + \frac{B}{x} = 0 \tag{A1}$$

with $u = x'(t)$, applying the chain rule $du/dt = (du/dx)(dx/dt) = u(du/dx)$, Eq. (A1) becomes,

$$\frac{du}{dx} + A = -\frac{B}{ux} \tag{A2}$$

Let $v = u + Ax$ then

$$\frac{dv}{dx} = \frac{du}{dx} + A = -\frac{B}{ux} = -\frac{B}{(v - Ax)x} \tag{A3}$$

Eq. (A3) can be written as:

$$\frac{dx}{dv} = \frac{Ax^2}{B} - \frac{vx}{B} \tag{A4}$$

Eq. (A4) is a Riccati equation. With the substitution $x = -Aw'/Bw$

$$\frac{dx}{dv} = -\frac{Aw''}{Bw} + \frac{A(w')^2}{Bw^2} = \frac{A(w')^2}{Bw^2} + \frac{vw'}{Bw} \tag{A5}$$

Eq. (A5) becomes,

$$w'' + \frac{vw'}{A} = 0 \tag{A6}$$

The solution for Eq. (A6) is

$$w' = C_1 e^{-\frac{Av^2}{2}} \tag{A7}$$

Therefore, solving for "w" yields,

$$w = C_2 + C_1 \int_0^v e^{-\frac{Av^2}{2}} dv \tag{A8}$$

Hence

$$x(v) = -\frac{Aw'}{Bw} = -\frac{AC_1 e^{-\frac{Av^2}{2}}}{B\left(C_2 + C_1 \int_0^v e^{-\frac{Av^2}{2}} dv\right)} = -\frac{Ae^{-\frac{Av^2}{2}}}{B\left(C + \int_0^v e^{-\frac{Av^2}{2}} dv\right)} \tag{A9}$$

C_1, C_2, C are arbitrary constants where $C = C_2/C_1$.
Deriving both sides of $v = u + Ax$ with respect to t gives

$$\frac{dv}{dt} = \frac{du}{dt} + A\frac{dx}{dt} = x''(t) + Ax'(t) = -\frac{B}{x} \tag{A10}$$

Thus

$$\frac{dt}{dv} = -\frac{x}{B} = \frac{Aw'}{B^2 w} \tag{A11}$$

From Eq. (A11) to acquire:

$$t(v) = \frac{A}{B^2} \ln w + C_3 = \frac{A}{B^2} \ln\left(C_2 + C_1 \int_0^v e^{-\frac{Av^2}{2}} dv\right) + C_3 = \frac{A}{B^2} \ln\left(C + \int_0^v e^{-\frac{Av^2}{2}} dv\right) + C^* \tag{A12}$$

where $C^* = (A/B^2)\ln C_1 + C_3$.
The solution for Eq. (A1) in the parametric form is

$$x(v) = -\frac{Ae^{-\frac{Av^2}{2}}}{B\left(C + \int_0^v e^{-\frac{Av^2}{2}} dv\right)} \tag{A13}$$

where the integral relates to time t by

$$t(v) = \frac{A}{B^2} \ln\left(C + \int_0^v e^{-\frac{Av^2}{2}} dv\right) + C^* \tag{A14}$$

where the integral can be evaluated using error function expressed by

$$\text{erf}\left(\sqrt{\frac{A}{2}}v\right) = \frac{2}{\sqrt{\pi}}\int_0^v e^{-\frac{Av^2}{2}}\,\mathrm{d}v \tag{A15}$$

Appendix B. Numerical formulation for mass transfer in spontaneous imbibition processes

The governing equation is

$$\frac{\mathrm{d}^2x}{\mathrm{d}t^2} + \frac{16\mu}{\rho d_H^2}\frac{\mathrm{d}x}{\mathrm{d}t} - \frac{p_c}{\rho x^2} = 0 \tag{B1}$$

which is simplified to

$$\frac{\mathrm{d}^2x}{\mathrm{d}t^2} + A\frac{\mathrm{d}x}{\mathrm{d}t} + \frac{B}{x} = 0 \tag{B2}$$

where,

$$A = \frac{16\mu}{\rho d_H^2},\ B = -\frac{p_c}{\rho} \tag{B3}$$

Using finite difference approximation we get,

$$\frac{x_{t+\Delta t} - 2x_t + x_{t-\Delta t}}{\Delta t^2} + \frac{A(x_{t+\Delta t} - x_{t-\Delta t})}{2\Delta t} + \frac{B}{x_t} = 0$$

$$\left(\frac{1}{\Delta t^2} + \frac{A}{2\Delta t}\right)x_{t+\Delta t} - \left(\frac{2x_t}{\Delta t^2} - \frac{B}{x_t}\right) + \left(\frac{1}{\Delta t^2} - \frac{A}{2\Delta t}\right)x_{t-\Delta t} = 0 \tag{B4}$$

$$\left(\frac{1}{\Delta t^2} - \frac{A}{2\Delta t}\right)x_{t-\Delta t}x_t - \frac{2x_t^2}{\Delta t^2} + \left(\frac{1}{\Delta t^2} + \frac{A}{2\Delta t}\right)x_t x_{t+\Delta t} + B = 0$$

Boundary conditions:

Eq. (B2) can be solved using the following conditions:

$$x_{t=0} = x_0 \quad \text{at} \quad t = 0$$

$$\left.\frac{\mathrm{d}x}{\mathrm{d}t}\right|_{t=0} = v_0 \quad \text{at} \quad t = 0 \tag{B5}$$

$$\frac{x_{\Delta t} - x_{-\Delta t}}{2\Delta t} = v_0$$

$$x_{-\Delta t} = x_{\Delta t} - 2v_0\Delta t$$

Let us consider t starting with "0" and t ends with t_{end}. We divide time with "n" intervals to get $\Delta t = (t_{end} - 0)/n$ or $t_{end} = n\Delta t$. We denote $t = 0$ by t_0, $t = \Delta t$ by t_1, $t = 2\Delta t$ by t_2s. Then $t_n = n\Delta t = t_{end}$ and in general $t_i = i\Delta t$.

Regarding x, we denote $x(t = i\Delta t = t_i)$ by x_i, then Eq. (B5) can be writen as

$$x_{-1} = x_1 - 2v_0\Delta t \tag{B6}$$

Now we write Eq. (B4) as

$$\left(\frac{1}{\Delta t^2} - \frac{A}{2\Delta t}\right)x_{i-1}x_i - \frac{2x_i^2}{\Delta t^2} + \left(\frac{1}{\Delta t^2} + \frac{A}{2\Delta t}\right)x_i x_{i+1} + B = 0 \tag{B7}$$

Let us write Eq. (B7) for every "t" to form a system of non-linear equations:

For $t = 0$,

$$\left(\frac{1}{\Delta t^2} - \frac{A}{2\Delta t}\right)x_{-1}x_0 - \frac{2x_0^2}{\Delta t^2} + \left(\frac{1}{\Delta t^2} + \frac{A}{2\Delta t}\right)x_0 x_1 + B = 0$$

$$-\left(\frac{1}{\Delta t^2} - \frac{A}{2\Delta t}\right)(x_1 - 2v_0\Delta t)x_0 - \frac{2x_0^2}{\Delta t^2} + \left(\frac{1}{\Delta t^2} + \frac{A}{2\Delta t}\right)x_0 x_1 + B = 0 \tag{B8}$$

For $t = \Delta t$,

$$\left(\frac{1}{\Delta t^2} - \frac{A}{2\Delta t}\right)x_0 x_1 - \frac{2x_1^2}{\Delta t^2} + \left(\frac{1}{\Delta t^2} + \frac{A}{2\Delta t}\right)x_1 x_2 + B = 0 \tag{B9}$$

For $t = 2\Delta t$,

$$\left(\frac{1}{\Delta t^2} - \frac{A}{2\Delta t}\right) x_1 x_2 - \frac{2x_2^3}{\Delta t^2} + \left(\frac{1}{\Delta t^2} + \frac{A}{2\Delta t}\right) x_2 x_3 + B = 0 \tag{B10}$$

$$\cdots$$

In this way, for $t = (n-1)\Delta t$,

$$\left(\frac{1}{\Delta t^2} - \frac{A}{2\Delta t}\right) x_{n-2} x_{n-1} - \frac{2x_{n-1}^2}{\Delta t^2} + \left(\frac{1}{\Delta t^2} + \frac{A}{2\Delta t}\right) x_{n-1} x_n + B = 0 \tag{B11}$$

Let

$$\frac{1}{\Delta t^2} - \frac{A}{2\Delta t} = c$$
$$\frac{2}{\Delta t^2} = d \tag{B12}$$
$$\frac{1}{\Delta t^2} + \frac{A}{2\Delta t} = e$$

The system of non-linear equation becomes:

$$-2cv_0\Delta t x_0 - dx_0^2 + dx_0 x_1 + B = 0 \tag{B13}$$

$$cx_0 x_1 - dx_1^2 + ex_1 x_2 + B = 0 \tag{B14}$$

$$cx_1 x_2 - dx_2^2 + ex_2 x_3 + B = 0 \tag{B15}$$

$$cx_2 x_3 - dx_3^2 + ex_3 x_4 + B = 0 \tag{B16}$$

$$\cdots$$

$$cx_{n-2} x_{n-1} - dx_{n-1}^2 + ex_{n-1} x_n + B = 0 \tag{B17}$$

For example, if $t_0 = 0$, $t_n = 1$, $\Delta t = 0.1$, then $n = 10$ and we have
$$t_0 = 0, \ t_1 = 0.1, \ t_2 = 0.2, \ t_3 = 0.3, \ t_4 = 0.4, \ t_5 = 0.5, \ \cdots, \ t_9 = 0.9, \ t_{10} = 1.0$$

Therefore,
$$x(t_0) = x_0, \ x(t_1) = x_1, \ x(t_2) = x_2, \ \cdots, \ x(t_9) = x_9, \ x(t_{10}) = x_{10}$$

We then have
$$-2cv_0\Delta t x_0 - dx_0^2 + dx_0 x_1 + B = 0$$
$$cx_0 x_1 - dx_1^2 + ex_1 x_2 + B = 0$$
$$cx_1 x_2 - dx_2^2 + ex_2 x_3 + B = 0$$
$$cx_2 x_3 - dx_3^2 + ex_3 x_4 + B = 0$$
$$cx_3 x_4 - dx_4^2 + ex_4 x_5 + B = 0$$
$$cx_4 x_5 - dx_5^2 + ex_5 x_6 + B = 0$$
$$cx_5 x_6 - dx_6^2 + ex_6 x_7 + B = 0$$
$$cx_6 x_7 - dx_7^2 + ex_7 x_8 + B = 0$$
$$cx_7 x_8 - dx_8^2 + ex_8 x_9 + B = 0$$
$$cx_8 x_9 - dx_9^2 + ex_9 x_{10} + B = 0$$

Now any numerical method can be used to solve this system of equation for $x_1, x_2, x_3, \cdots, x_{10}$.